Influence of probe geometry on measurement results of non-ideal thermal conductivity sensors

P. Tiefenbacher, N. I. Kömle, W. Macher, and G. Kargl

Space Research Institute, Austrian Academy of Sciences, Graz, Austria

Correspondence to: P. Tiefenbacher (patrick.tiefenbacher@oeaw.ac.at)

Abstract. The thermal properties of the surface and subsurface layers of planets and planetary objects yield important information that allows us to better understand the thermal evolution of the body itself and its interactions with the environment. Various planetary bodies of our Solar System are covered by so-called regolith, a granular and porous material. On such planetary bodies the dominant heat transfer mechanism is heat conduction via IR radiation and contact points between particles. In this case the energy balance is mainly controlled by the effective thermal conductivity of the top surface layers, that can be directly measured by thermal conductivity probes. A traditionally used method for measuring the thermal conductivity of solid materials is the needle-probe method. Such probes consist of thin steel needles with an embedded heating wire and temperature sensors. For the evaluation of the thermal conductivity of a specific material the temperature change with time is determined by heating a resistance wire with a well-defined electrical current flowing through it and simultaneously measuring the temperature increase inside the probe over a certain time. For thin needle probes with a large length-to-diameter ratio it is mathematically easy to derive the thermal conductivity, while this is not so straightforward for more rugged probes with a larger diameter and thus a smaller length-to-diameter ratio. Due to the geometry of the standard thin needle probes they are mechanically weak and subject to bending when driven into a soil. Therefore, using them for planetary missions can be problematic.

In this paper the thermal conductivity values determined by measurements with two non-ideal, ruggedized thermal conductivity sensors, which only differ in length, are compared to each other. Since the theory describing the temperature response of non-ideal sensors is highly complicated, those sensors were calibrated with an ideal reference sensor in various solid and granular materials. The calibration procedure and the results are described in this work.

1 Introduction

One way for a better understanding of our solar system is a better knowledge of the objects in it, the planets and their satellites, as well as asteroids and comet nuclei. An important part of this knowledge are the physical properties of their surface layers, i.e. mechanical, optical, electrical and thermal properties. The last ones are in the focus of this work. Thermal conductivity of the materials composing the solid near-surface layers of the planetary bodies mentioned above is of high interest for the following reasons. One reason is that for modelling the thermal evolution of any planetary body the average heat flux across the surface is an important boundary condition (Hofmeister et al., 2007). Another reason for the importance of measuring these thermal properties is that they control, together with the other physical properties mentioned above, the processes on

a planetary surface to a high extent (Kömle, 2005). Moreover, variations in thermal conductivity can be an indicator for the presence of water-saturated soil or ice, because dry soil has a significantly smaller thermal conductivity than wet soil or ice (Incropera et al., 2007).

However, measurements of thermal properties on planetary bodies, except of the Earth, are still scarce. To date only for two terrestrial bodies - Moon and Mars - thermal properties have been measured in situ. Apollo 15 (1971) and Apollo 17 (1972) carried experiment packages, called ALSEP, for measuring the thermal conductivity and the vertical temperature gradient on the Moon (Langseth et al., 1972), (Langseth et al., 1973). The first in situ measurements of thermal properties on Mars were carried out by the *Thermal and Electrical Conductivity Probe (TECP)* on board the lander Phoenix in 2008 (Zent et al., 2010). So there is a need for geophysical in situ exploration of the subsurface in future lander missions for prospecting water ice and water deposits or other resources. For example, such instruments might be part of the payload for the upcoming Russian Lunar Polar Lander missions, which have the goal to investigate the properties of the regolith in the lunar south polar regions by in situ measurements and by returning samples to Earth (ESA, 2014). These areas are of particular interest, because they are expected to contain water ice at shallow depths.

In the middle of the last century one can find the first theoretical descriptions and experiments concerning so called single-probes. They are described among others by (Blackwell, 1952) and (Blackwell, 1954). For the *Single-Probe Method* a single needle-probe is used, which at the same time serves as a heater and as a sensor for measuring temperature. The basic principle of this method is to heat the cylindrical probe embedded in the respective sample material by a constant power supply for a defined time interval, while the temperature response is measured simultaneously. The thermal properties of the surrounding medium are influencing the measured temperature increase in a way that allows their determination from the measured temperature response.

For the thermal conductivity measurements we make use of various needle sensors built by the Dutch company Hukseflux. The model TP02 (Hukseflux, 2010) serves as the standard reference sensor. It is used to calibrate other custom-made models (denoted as LNP03 and LNP04), which are mechanically more robust and therefore may be better suited to be used as a payload for planetary surface missions than standard probes. This work lays the basis for further investigations on the effects of probe geometry and thus makes a significant contribution towards the development of a reliable thermal properties instrument for future planetary lander missions.

In the following sections one can find the theoretical approach for needle-shaped thermal sensors, a short presentation of the used measurement probes, the results of thermal conductivity measurements in various sample materials, as well as the calibration of the LNP sensors and a comparison between LNP03 and LNP04.

2 Theory of non-ideal thermal sensors

Generally there a two main groups of thermal conductivity measurement methods.

On the one hand the *steady-state methods*, where an over time constant temperature difference is established. For these methods a complex and expensive measurement system is needed. Therefore these methods are not optimal for field and space

applications.

On the other hand the *non-steady-state* or *transient methods*, where usually a needle-shaped heater embedded in a sample is heated over a certain time interval and the temperature response, which depends on the thermal properties of the sample, is measured at or near the heater at the same time. Due to the smaller complexity and costs of these systems they are more suitable for field and space applications. For measurements done for this work a transient method using needle shaped heater/sensor combinations with different geometry was chosen. The theory of this method is outlined below. All parameter and variables in the equations mentioned in this section are listed and explained in Table 1.

Table 1. Parameters and variables of the equations used for the theoretical approach.

T	[K]	...temperature
T_0	[K]	...ambient temperature
t	[s]	...characteristic time
r	[m]	...radial distance from the center
r_{sen}	[m]	...sensor radius
Q	[Wm^{-3}]	...volume power density
Q_l	[Wm^{-1}]	...power per length
k	[Wm^{-1}K^{-1}]	...thermal conductivity, sample
κ	[m^{2}s^{-1}]	...thermal diffusivity, sample
ρ	[kgm^{-3}]	...density, sample
c_p	[Jkg^{-1}K^{-1}]	...specific heat capacity, sample
S	[Jm^{-1}K]	...heat capacity per length, sensor
H	[Wm^{-2}K^{-1}]	...thermal contact conductance sensor/sample

2.1 Transient thermal conductivity probes

According to (Carslaw and Jaeger, 1959) an infinite line heat source placed in an infinite, homogeneous and isotropic medium is the general approach for the line heat source technique. As described in (Özisik, 1989) the heat conduction equation of such a cylinder-symmetric, one-dimensional boundary value problem can be written as

$$\frac{\partial^2 T}{\partial r^2} + \frac{1}{r}\frac{\partial T}{\partial r} + \frac{Q(r,t)}{k} = \frac{1}{\kappa}\frac{\partial T}{\partial t}; \quad 0 \le r < \infty, \, t > 0, \tag{1}$$

where r is the radial distance from the center. $Q(r,t)$ [Wm^{-3}] denotes a volume heat source. The following initial and boundary conditions are to be satisfied:

$$T = T_0 \quad \text{for} \quad \begin{cases} 0 \le r < \infty, \, t = 0 \\ r \to \infty, \, t > 0 \end{cases}$$

A general solution can be obtained by integral transform, in this case a Hankel transform (Özisik, 1989):

$$T(r,t) = T_0 + \int_{\beta=0}^{\infty} \beta J_0(\beta r) \exp(-\kappa\beta^2 t) \left[\frac{\kappa}{k} \int_{t'=0}^{t} \exp(\kappa\beta^2 t') dt' \int_{r'=0}^{\infty} r' J_0(\beta r') Q(r',t') dr' \right] d\beta, \tag{2}$$

where J_0 is the Bessel function of the first kind and of order zero.

2.1.1 Infinite line heat source with neglected sensor properties

For many applications it is sufficient to consider an infinite line heat source Q_l [Wm^{-1}] immersed in an infinite medium positioned at $r=0$. Being aware that in practice the heat source can not be a perfect line and that neither the heat source nor the surrounding medium is infinite various errors arise from this idealization. Nevertheless, this approach allows a good first estimate of the thermal conductivity of the respective medium, as will be described below. For an infinite line heat source Q_l positioned in the center ($r=0$) that supplies energy at a constant rate, the volume power density $Q(r,t)$ [Wm^{-3}] can be defined as:

$$Q(r,t) = \frac{Q_l}{2\pi r}\delta(r-0), \tag{3}$$

where $\delta(r-0)$ is the Dirac delta function at $r=0$. By substituting Eq. (3) into Eq. (2) an expression for the temperature response to the heat emitted from the line heat source is obtained:

$$T(r,t) = T_0 + \frac{1}{4\pi k} \int_{t'=0}^{t} \frac{Q_l(t)}{(t-t')} \exp\left(\frac{-r^2}{4\kappa(t-t')}\right) dt', \tag{4}$$

and for $Q_l = $ const.:

$$T(r,t) = T_0 + \frac{Q_l}{4\pi k} \int_{\frac{r^2}{4\kappa t}}^{\infty} \frac{\exp(-u)}{u} du = T_0 + \frac{Q_l}{4\pi k} E_1\left(\frac{r^2}{4\kappa t}\right), \tag{5}$$

where $E_1(x) = \int_x^{\infty} \frac{\exp(-u)}{u} du$ is denoted as *exponential integral function*, which is defined as a particular definite integral of the ratio between an exponential function and its argument. As described in (Abramowitz and Stegun, 1964) this integral can also be expressed by a series expansion:

$$E_1(x) = -\gamma - \ln x - \sum_{n=1}^{\infty} \frac{(-1)^n x^n}{n n!}$$

$$= -\gamma - \ln x + x - \frac{1}{4}x^2 + \mathcal{O}(x^3). \tag{6}$$

The constant $\gamma = 0.5772...$ is known as the Euler-Mascheroni constant or Euler's constant. The contributions in Eq. (6) after the logarithmic term can be neglected for small x-values (equivalent to large t-values). Thus, using Eq. (5) and Eq. (6) the temperature change can be approximated by

$$T(r,t) - T_0 = \frac{Q_l}{4\pi k}\left[-\gamma + \ln t + \ln\left(\frac{4\kappa}{r^2}\right) + ... \right]. \tag{7}$$

Furthermore, the variation of temperature with the natural logarithm of time, $\ln t$, as the independent variable can be written as

$$\frac{dT}{d\ln t} = \frac{Q_l}{4\pi k}. \tag{8}$$

This formular shows that, after an initial non-linear temperature rise a linear relationship between the probe temperature and the natural logarithm of time is established. With knowledge of the heating power and the temperature increase as a function of time the thermal conductivity can be derived from Relation (8):

$$k = \frac{Q_l}{4\pi} \left(\frac{dT}{d\ln t} \right)^{-1}. \tag{9}$$

An improvement over this idealized geometry is the determination of a heat source of finite radius in a similar analytical way as described below. Moreover, in (Hütter and Kömle, 2012) it is explained that the evaluation approach for a line heat source can also be used for large hollow cylindrical geometries if measurement time is long enough.

2.1.2 Heat source with thermal surface resistance and non-ideal sensor properties

The theory presented in the previous section is idealized in various ways. It is assumed that the heat source is concentrated in a line and that there is negligible sensor heat capacity and thermal conductance across the probe-sample interface. However, this is not the case for real probes. Every real sensor has finite dimensions and characteristic thermal properties differing from the sample properties. Furthermore, there exists a more or less high thermal contact resistance at the boundary between sensor and sample material, depending on composition and structure of the sample.

Solutions of the heat equation for this problem have been developed amongst others by (Jaeger, 1956). These relations include a non-negligible heat capacity of the sensor S [$\mathrm{Jm^{-1}K^{-1}}$] and a finite thermal contact conductance H [$\mathrm{Wm^{-2}K^{-1}}$][1]. S is the specific volumetric heat capacity of the sensor material per sensor length multiplied by the sensor cross section:

$$S = c_{sen}\rho_{sen}A_{sen}. \tag{10}$$

The general solution, Eq. (14), can be derived by introducing three dimensionless variables, where all the basic parameters of the problem are included:

$$\tau = \frac{\kappa t}{r_{sen}^2}, \tag{11}$$

$$\alpha = \frac{2\pi r_{sen}^2 \rho c_p}{S}, \tag{12}$$

$$h = \frac{k}{r_{sen}H}. \tag{13}$$

---

[1]Thermal resistance is the inverse of thermal conductance H, i.e $H \to \infty$ is equivalent to $(1/H) \to 0$ (there is no temperature discontinuity across the respective boundary) (Incropera et al., 2007).

τ is called *Fourier number* and it represents the characteristic time for the propagation of the heat wave originating from a heated cylinder with radius r_{sen} in the surrounding medium.

α represents the ratio of the sample heat capacity to that of the sensor.

h is proportional to the ratio of the sample conductivity to the thermal surface conductance between sensor and surrounding

5 sample.

Assuming that the thermal conductivity of the sensor probe is large compared to that of the sample material, that the cylinder is in thermal equilibrium with the surrounding medium at $t = 0$ ($T(r, 0) = 0$) and that heat is supplied at the rate per unit length Q_l for a defined time interval to the cylinder core, the temperature T in the core at time t is given by the following formula

10 (Jaeger, 1956):

$$T = G(h, \alpha, \tau) = \frac{2Q_l \alpha^2}{k\pi^3} \int\limits_0^\infty \frac{[1 - \exp(-\tau u^2)]}{u^3 f(u)} du \tag{14}$$

with

$$f(u) = \left[uJ_0(u) - (\alpha - hu^2)J_1(u) \right]^2 + \left[uY_0(u) - (\alpha - hu^2)Y_1(u) \right]^2. \tag{15}$$

J_0 and J_1 are the regular Bessel functions of the first kind and of order zero and one, respectively, Y_0 and Y_1 are the Bessel

15 functions of the second kind and of order zero and one. For small values of τ the so-called short time approximation is obtained:

$$T_{short\text{-}t} = \frac{Q_l \alpha}{2\pi k} \left[\tau - \frac{\alpha \tau^2}{2h} + \mathcal{O}\left(\tau^{\frac{5}{2}}\right) \right], \quad \text{if } h \neq 0, \tag{16a}$$

$$\text{or} \quad T_{short\text{-}t} = \frac{Q_l \alpha}{2\pi k} \left[\tau - \frac{4\alpha}{3\pi^{\frac{1}{2}}} \tau^{\frac{3}{2}} + \mathcal{O}\left(\tau^2\right) \right], \quad \text{if } h = 0. \tag{16b}$$

For large values of τ the long time approximation is obtained:

20 $$T_{long\text{-}t} = \frac{Q_l}{4\pi k} \left[2h + \ln\left(\frac{4\tau}{C}\right) - \frac{(4h - \alpha)}{2\alpha\tau} + \frac{(\alpha - 2)}{2\alpha\tau} \ln\left(\frac{4\tau}{C}\right) + ... \right], \tag{17}$$

where $C = \exp(\gamma) = 1.7811...$ with Euler's constant $\gamma = 0.5772....$ Eq. (17) becomes Eq. (7) (when the initial temperature is set to zero) for the case of a very thin sensor and vanishing thermal contact resistance between sensor probe and sample material. It follows from Formula (17) that a plot of T against $\ln t$ has a linear asymptote of slope $Q_l/(4\pi k)$ and so k can be determined immediately if Q_l is known.

25 Furthermore, in (Macher et al., 2013) another interesting case for the development of thermal conductivity sensors is studied, which will not be discussed here. They considered temperature evolution in and around a heated infinite cylinder with a tubular sheath, assuming non-negligible surface resistances between core and sheath of the cylinder and between the sheath and the surrounding medium.

2.2 Data evaluation

The characteristic temperature response of a linear heat source (T vs. $\ln t$) to heating is shown in Fig. 1 after (Jones, 1988).
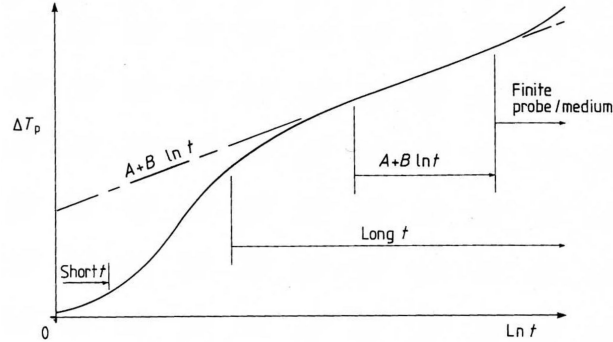
Figure 1. Qualitative heating curve measured with a line heat sensor (Jones, 1988).

Four main segments can be identified in this curve. The initial phase after the onset of heating can be used for the evaluation of the thermal conductiviy of the sample by the so-called short time approximation (Eq. (16a)). It is followed by the non-linear

5 second segment, where self-heating of the probe and contact resistance between probe and sample material are dominating and thus this approximation is no longer valid. The end of this segment is defined by a transition to the linear portion where T depends linearly on $\ln t$. With respect to time this is the section between transient time and maximal measurement time defined in Sect. 2.2.1. This part of the curve is used for the evaluation of the thermal conductivity of the sample by linear regression. (Jones, 1988) and others used a non-linear long time approximation for the heating curve. They considered a probe with finite

10 diameter and non-negligible contact resistance between probe and sample material. The non-linear equation is equivalent to Eq. (17) and reads as follows:

$$T = A + B\ln t + C\frac{\ln t}{t} + D\frac{1}{t} + \mathcal{O}\left(\frac{\ln t}{t^2}\right), \tag{18}$$

with the coefficients

$$A = \frac{Q_l}{4\pi k}\left[\ln\left(\frac{4\kappa}{r_{sen}^2}\right) - \gamma + \frac{2k}{r_{sen}H}\right] = \frac{Q}{4\pi k}X, \tag{19a}$$

15 $$B = \frac{Q_l}{4\pi k}, \tag{19b}$$

$$C = \frac{Q_l}{4\pi k}\frac{r_{sen}^2}{2\kappa}\left(1 - \frac{\kappa S}{\pi r_{sen}^2 k}\right), \tag{19c}$$

$$D = \frac{Q_l}{4\pi k}\frac{r_{sen}^2}{2\kappa}\left[\ln\left(\frac{4\kappa}{r_{sen}^2}\right) + (1 - \gamma) - \frac{\kappa S}{\pi r_{sen}^2 k}X\right]. \tag{19d}$$

The second term of Eq. (18) with the coefficient B, given in Relation (19b), is equivalent to Eq. (8). From this formula the thermal conductivity k can be easily determined. The other terms of the equation with their respective coefficients can be used to evaluate the other unknown parameters of the sensor probe and the sample. These are the thermal diffusivity κ of the sample, the surface conductance H between probe and sample and the heat capacity per unit length S of the sensor. The last segment of

5 the curve, beginning at the maximum measurement time, is non-linear again, due to finite sample dimensions and axial errors. (Hütter, 2011) describes two different behaviours of the curve in this last section, providing information about the measurement system. An increasing curve can be observed if the heat wave reaches the wall of the sample container and its conductivity is lower than that of the sample. A decrease of the curve in this section can be observed if convection starts to play a role or if the conductivity of the sample container wall is higher than that of the sample.

10 Temperature–time data, the heating current and the heater resistance are necessary input data for the evaluation of thermal conductivity. This information, together with the estimated transient and maximum measurement times, were integrated into an evaluation program, written in MATLAB.

2.2.1 Time period for evaluation

Due to the non-ideal measurement conditions there are some limitations for the evaluation that have to be considered. The

15 thermal diffusivity κ of the sample to be measured and the geometric dimensions of the respective sample and sensor are the key parameters. Two characteristic times can be defined and should be estimated before the measurement:

The **transient time** t_{trans} is the time from the onset of heating ($t = 0$) until the beginning of the linear part of the T-$\ln t$ curve (see Fig. 1). This time can be estimated according to (Goodhew and Griffiths, 2004) as

$$t_{trans} = \frac{50 r_{sen}^2}{4\kappa}, \qquad (20)$$

20 where r_{sen} is the radius of the sensor probe. This formula is valid for a full cylinder with radius r_{sen}.

The **maximum measurement time** t_{max} is the other characteristic time. It is caused by the finite dimension of the sample containers in laboratory measurements. The reason for the existence of this upper time limit is that the heat wave originating from the needle probe reaches the boundary of the sample container after some time, depending on the thermal properties of the respective sample and the distance of the sensor from the boundary. The boundary condition stated in Sect. 2.1, $T = T_0$

25 as $r \rightarrow \infty$, is violated when the thermal wave reaches the boundary of the sample container. Therefore it must always be made sure that the duration of one measurement does not exceed t_{max}. Once the heat wave is reflected from the boundaries, the temperature profile is influenced in a way not included in the theory. According to (Goodhew and Griffiths, 2004) the maximum measurement time can be estimated by the formula:

$$t_{max} = \frac{0.6(r_{sample} - r_{sen})^2}{4\kappa}. \qquad (21)$$

30 ### 2.2.2 Error assessment

There are numerous error sources which are responsible for the uncertainty of the thermal conductivity determined by the various sensors. For the estimation of an overall error the laws of error propagation were used. Generally the resulting quantity

y of an experiment is a function of several measured variables x_i:

$$y = f(x_i). \tag{22}$$

Variations of the variables x_i causes the error dy of y, which can be expressed as

$$dy = \sum \frac{\partial y}{\partial x_i} dx_i. \tag{23}$$

5   The focus of this work is the evaluation of the thermal conductivity. The function $f(x_i)$ is the relation used for this calculation, defined as

$$k(Q,s) = \frac{Q}{4\pi s}. \tag{24}$$

The parameter s denotes the slope of the linear part of the measurement curve when the measured temperature T is plotted against $\ln t$, which is used for the evaluation. Equation (24) can be rewritten in terms of the measurement parameters:

10    $$k = \frac{RI_{heat}^2}{4\pi} \frac{\Delta \ln t}{\Delta T}, \tag{25}$$

where $R \, [\Omega \mathrm{m}^{-1}]$ is the electrical resistance per unit length of the heating wire of the respective sensor needle and $I_{heat} \, [\mathrm{A}]$ is the applied constant heating current. Based on Relation (23) the variation of the thermal conductivity k due to variations of the measured quantities can be written as

$$\delta k = \frac{\partial k}{\partial R} \delta R + \frac{\partial k}{\partial I_{heat}} \delta I_{heat} + \left(\delta \frac{d\ln t}{dT} \right) \left(\frac{RI^2}{4\pi} \right). \tag{26}$$

15   Evaluation of Eq. (26) according to Relation (23) leads to the relative error for the thermal conductivity measurement:

$$\frac{\delta k}{k} = \frac{\delta R}{R} + 2\frac{\delta I_{heat}}{I_{heat}} - \frac{\delta \left(\frac{dT}{d\ln t} \right)}{\frac{dT}{d\ln t}}. \tag{27}$$

The form $\frac{dT}{d\ln t}$ describes the slope of the T-$\ln t$ curve from linear regression and is denoted in the following by:

$$\mu = \frac{dT}{d\ln t}. \tag{28}$$

With this definition the last term of Eq. (27) can be approximated as

20    $$-\frac{\delta \mu}{\mu} = \left(\frac{\delta t_2}{t_2} - \frac{\delta t_1}{t_1} \right) \frac{1}{\ln t_2 - \ln t_1} - \frac{\delta T_2 - \delta T_1}{T_2 - T_1}. \tag{29}$$

The subscripts behind the parameters T and t describe points on the T-$\ln t$ curve, where 1 corresponds to the point at the beginning of the linear part of the curve and 2 corresponds to the end of the linear part (compare Fig. 1). The following two assumptions can be made:

First, the error of the measurement time can be neglected:

25    $$\delta t_1 \approx \delta t_2 \approx 0. \tag{30}$$

Second, the temperature error for the temperature values at the beginning of the linear part of the T-$\ln t$ curve is assumed to be approximately the same as for the values at the end of the linear part of the curve and is defined as

$$|\delta T_1| \approx |\delta T_2| \equiv \delta T. \tag{31}$$

So Eq. (29) can be rewritten as

$$\frac{|\delta \mu|}{\mu} = 2\frac{\delta T}{T_2 - T_1}. \tag{32}$$

With this simplification and since all the measurement errors are independent of each other Eq. (27) yields:

$$\frac{|\delta k|}{k} = \sqrt{\left(\frac{\delta R}{R}\right)^2 + \left(2\frac{\delta I}{I}\right)^2 + \left(2\frac{\delta T}{T_2 - T_1}\right)^2}. \tag{33}$$

The third term in this formula shows the relative temperature error, which is the ratio of the error of the temperature measurement to the temperature increase in the linear regime. It can be seen that the relative error is linked to the slope of the

10 measurement curve: The bigger the temperature difference $(T_2 - T_1)$, the steeper is the slope and the smaller the relative temperature error. The gradient of the increase of the slope depends on the sample material.

If linear regression is applied, the following form can be used for the evaluation of the relative error of thermal conductivity:

$$\frac{|\delta k|}{k} = \sqrt{\left(\frac{\delta R}{R}\right)^2 + \left(2\frac{\delta I}{I}\right)^2 + \left(\frac{\delta \mu}{\mu}\right)^2}, \tag{34}$$

where the resulting slope and its error from the regression (of the T-$\ln t$ curve) are substituted for μ and $\delta\mu$. The variation of

15 the thermal conductivity is caused by the variations of the heater resistance R, the heating current I_{heat} and the uncertainties of the measured temperature T (or of the slope μ from regression), as given in Eq. (33) and Eq. (34). Generally all these variations consist of uncertainties from needle probe fabrication, used temperature sensors and uncertainties from power supply and data acquisition unit. The maximum possible deviation of a parameter is evaluated by summing up all the variations influencing the measurement. In Eq. 34 for error propagation δR, δI and $\delta\mu$ are the result of bias (systematic errors) as well as measurement

20 errors, as indicated in the following, where the most important error sources are described:

Resistance error ($\delta\mathbf{R}$): The resistance of the heating wire cannot be measured continuously, so the measurement precision of a typical digital multimeter used for measuring the resistance is taken into account (see Table 2). The heating wires embedded in all sensors are made of the alloy constantan, which has a constant resistance of 49 μΩ at temperatures between 20 °C and 500 °C (Heusler, 2014). Therefore the bias caused by the change of resistance with temperature is negligible.

25 **Heating current error** ($\delta\mathbf{I}$): The constant current flowing through the heating wire is generated by the TTi power supply and continuously measured by the Agilent data logger. Both devices are a source of measurement error. The first term in the $\frac{\delta I}{I}$ column in Table 2 is the measurement error caused by the data logger according to (Agilent, 2012) and the second term the measurement error caused by the power supply according to (TTi, 2003). These errors are determined for each measurement.

Time error ($\delta\mathbf{t}$): The time reading error was assumed to be negligible.

30 **Temperature error** ($\delta\mathbf{T}$): The temperature at the TP02 sensor is determined by a differential thermocouple measurement. The

reference temperature above the sample is measured by a Pt1000 resistance temperature detector (RTD), mounted in the base of the sensor, for establishing the absolute medium temperature. Due to the differential measurement of the two thermocouples there is no additional bias and the error is essentially due to the RTD resistance measurement. The Pt1000 RTD is also used in the LNP03 and LNP04 sensors. RTDs are sensors for measuring temperature in virtue of the correlation of the RTD resistance

5 with temperature. So the relative error of the temperature measurement is in the same order of magnitude as the relative error of the measured resistance. The errors caused by the Agilent data logger (Agilent, 2012) are taken into account (see Table 2), while the bias of the RTD can be neglected due to its small tolerance range at the given temperature.

Table 2. Error estimates of the quantities measured during thermal conductivity measurement, listed for the different sensors.

Sensor	$\frac{\delta \mathbf{R}}{\mathbf{R}}$	$\frac{\delta \mathbf{I}}{\mathbf{I}}$	$\frac{\delta \mathbf{T}}{\mathbf{T}}$ [1]
TP02	$\frac{\pm(0.0005 \cdot R + 0.1\ \Omega)}{R}$	$\frac{\pm(0.0005 \cdot I + 5 \times 10^{-6}\ \text{A}) \pm (0.002 \cdot I + 0.005\ \text{A})}{I}$	$\frac{\pm(0.0001 \cdot R + 0.01\ \Omega)}{R}$
LNP03	$\frac{\pm(0.0005 \cdot R + 0.1\ \Omega)}{R}$	$\frac{\pm(0.001 \cdot I + 0.0001\ \text{A}) \pm (0.002 \cdot I + 0.005\ \text{A})}{I}$	$\frac{\pm(0.0001 \cdot R + 0.01\ \Omega)}{R}$
LNP04	$\frac{\pm(0.0005 \cdot R + 0.1\ \Omega)}{R}$	$\frac{\pm(0.001 \cdot I + 0.0001\ \text{A}) \pm (0.002 \cdot I + 0.005\ \text{A})}{I}$	$\frac{\pm(0.0001 \cdot R + 0.01\ \Omega)}{R}$

[1] The relative error of the temperature measurement was calculated as the relative error of the resistance measurement as given in the Agilent data sheet (Agilent, 2012).

Finally, the scattering (variance) of the data points in the T-$\ln t$ curve contributes to the error $\frac{\delta \mu}{\mu}$ in Eq. 34. However, this contribution is much smaller than the error estimation $\frac{\delta T}{T}$ given in Table 2. Therefore Eq. (33) is used instead of Eq. (34),

10 providing a good estimate for the total relative error of each determined conductivity value (as indicated by error bars in the Fig. 8 to 13). In each figure the standard deviation σ, belonging to the respective measurement sequences, are given, calculated by

$$\sigma = \sqrt{\sum_{i=1}^{n} \frac{(x_i - \overline{x})^2}{n-1}} \qquad (35)$$

where n is the number of conductivity values x_i per sequence and $\overline{x}$ is their mean value. In fact, the variance of the conductivity

15 values (as plotted in these figures) is well represented by the estimated error bars (apart from some outliers which are to be expected from a statistical point of view).

3 Measurement probes

The thermal conductivity of the various samples was measured with different measurement probes. On the one hand a commercial thermal conductivity sensor, denoted as TP02, and on the other hand two different versions of custom-made sensors,

20 LNP03 and LNP04, all manufactured by the Dutch company Hukseflux, were used. The LNP sensors were designed to investigate their suitability for space application. They are shorter and thicker and therefore more rugged than the commercial TP02

sensor, which can be easily deformed by bending when used in granular material with larger grain sizes or in a material with internal cohesion. However, due to the smaller length-to-diameter ratio of the LNP probes the evaluation of thermal conductivity is not as straightforward as it is for the "optimal" line heat sources, described in the previous sections. Additional calibration is necessary. The LNP03 and the LNP04 sensors are constructed identically, except for their length. The LNP04 sensor is 20 mm shorter and thus a little more robust than the LNP03, but the length-to-diameter ratio is smaller. In the following the individual probes are described in more detail.

3.1 TP02

The TP02 sensor is a commercial non-steady-state probe (NSSP) for thermal conductivity measurement. The NSSP measurement method is also known as transient line heat source, thermal needle, hot needle, heat pulse- and hot wire technique as described in Sect. 2. Generally such a probe consists of a heating wire, representing a perfect line heat source and a temperature sensor capable of measuring the temperature at the heat source region. For investigation of a medium the probe is inserted into it. Measurements with the TP02 sensor are absolute, i.e. there is in principle no need for reference materials.

Three TP02 sensors were used for our measurements, which only differ in heater resistance. The sensor has a length of 150 mm and a diameter of 1.5 mm, which implies a length-to-diameter ratio of 66. According to (Kömle et al., 2013) sensors with a ratio of 60 or more fulfil the requirements for the evaluation based on line heat source theory, so the TP02 sensor meets this requirement. The uppermost 100 mm are actively heated by an embedded constantan heating wire. All described dimensions can be found in Fig. 3. For temperature measurement the sensor incorporates two thermocouple junctions (thermocouple type K) producing a voltage output that is proportional to ΔT between heated and unheated part. One positioned 50 mm from the base in the heated part, the other one in the unheated tip. Additionally a Pt1000 RTD in the base measures the surrounding temperature and enables the evaluation of the absolute medium temperature. The structure of the TP02 is shown in Fig. 2 and 3. This design provides optimal accuracy independent of the medium temperature and a minimal sensitivity to thermal gradients. The TP02 sensor was used as a reference sensor for calibration of the LNP03 sensor (Kömle et al., 2013) and the LNP04 sensor, as described in Sect. 5.
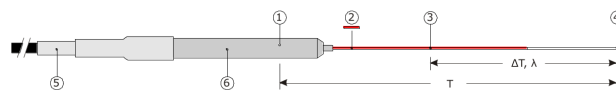
Figure 2. The TP02 probe consists of a needle with two thermocouple junctions; the hot joint (3), the cold joint (4) (remains at a stable temperature) and a heating wire (2). In the base (6) a reference temperature sensor (Pt1000) (1) is mounted. (Hukseflux, 2010)

For the evaluation of the thermal conductivity of a sample measured with the TP02 probe the thermocouple readings have to be converted from voltage into temperature. Therefore, as described in (Hukseflux, 2010), the temperature dependent sensitivity of the thermocouple E_{sen} [VK^{-1}] is calculated as

$$E_{sen} = 10^{-6}(a_0 + a_1 T - a_2 T^2),$$
(36)
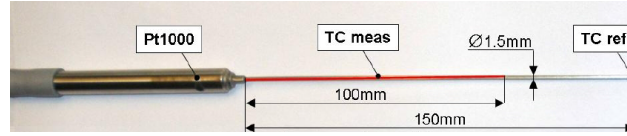
Figure 3. Commercial TP02 thermal conductivity probe (Hütter, 2011).

with the constants $a_0 = 39.40 \text{ VK}^{-1}$, $a_1 = 0.050 \text{ VK}^{-2}$ and $a_2 = 0.0003 \text{ VK}^{-3}$.

The Pt1000 RTD gives the temperature of the sensor's surroundings, so with its readings the absolute temperature T can be calculated. Temperature change measured close to the heating wire is then derived as

$$\Delta T = \frac{U_{sen}}{E_{sen}}, \tag{37}$$

where U_{sen} is the thermoelectric voltage generated at the thermocouple hot junction. According to (Hukseflux, 2010) the sensitivity given in Eq. (36) should be accurate within 1 % in the temperature range from -40 °C to 100 °C.

With the Pt1000 RTD resistance values are measured, which have to be converted into temperature values. The relation between resistance R and temperature T of platinum RTDs is described by the Callendar-van Dusen equation (McGee, 1988):

$$R = R_0 \left[1 + AT + BT^2 + CT^3(T - 100) \right], \tag{38a}$$

$$R = R_0 \left[1 + AT + BT^2 \right], \tag{38b}$$

where Eq. (38a) is valid for the temperature range of -200 °C to 0 °C and Eq. (38b) for the temperature range of 0 °C to 850 °C. The constants have the following values:

$$A = +3.9083 \times 10^{-3} \, °\text{C}^{-1},$$
$$B = -5.7750 \times 10^{-7} \, °\text{C}^{-2},$$
$$C = -4.1830 \times 10^{-12} \, °\text{C}^{-3}.$$

These equations and the values of the constants are especially valid for platinum RTDs, so no further calibration is necessary. If the RTD element is made from another material the constants A, B and C have to be determined separately (Schaffer, 2014).

3.2   LNP03

The LNP03 sensor is a custom-made prototype thermal conductivity sensor. There is one sensor, the LNP-A (further denoted as LNP03-needle 4), which has a mounting stud with a screw thread at the top for installing it onto a deployment device (for example a robotic arm on a planetary lander). In relation to the whole needle such a part has a relatively large mass and heat capacity and could therefore influence the measurements. Thus two identical sensors, the LNP-B (further denoted as LNP03-needle 2 and LNP03-needle 3), were built consisting only of the needle and the necessary heating and measurement parts without such a mounting stud, but with the same geometric dimensions. Both versions are shown in Fig. 4.

The sensor has a needle length of 100 mm and a diameter of 3.5 mm, which implies a length-to-diameter ratio of 28. This is far below the minimal ratio of 60 for evaluation on the basis of the line heat source theory, but the sensor is more robust than the TP02 sensor and can hardly be bended. For the heating of the LNP03 sensor a constantan wire is embedded in the needle, which extends over the whole needle length. The temperature response to heating is measured with three Pt1000 RTDs

5   placed at the following positions (see Fig. 4): close to the tip, in the center of the needle and close to the base of the needle. The conversion of the resistance values measured by the RTDs to temperature values is described in Sect. 3.1. Only the values of the middle sensor were used for the evaluation of the thermal conductivity. The temperature is measured with a 4-wire technique to increase the measurement accuracy.
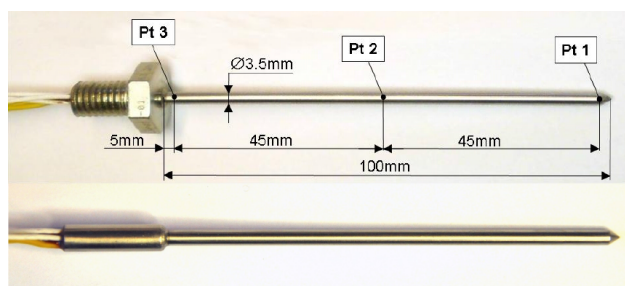
Figure 4. LNP03 thermal conductivity probe prototype. The upper picture shows the LNP-A, further denoted as LNP03-needle 4 and the lower picture shows the LNP-B, which is further denoted as LNP03-needle 2 and LNP03-needle 3.

3.3   LNP04

10   The LNP04 sensor is the further developed version of the LNP03 custom-made prototype and is shown in Fig. 5. The differences are the needle length and the construction of the mounting stud. There are four identical sensor needles in use. As the LNP-A, the LNP04 sensor is equipped with a mounting stud with a screw thread on the top for installing it onto a deployment device, but this one has less mass and thus less heat capacity which could influence the measurements.

    With a length of 80 mm the LNP04 sensor is 20 mm shorter than the LNP03 but has the same diameter, implying a length-

15   to-diameter ratio of 22. This is also far below the minimal ratio of 60 for evaluation on the basis of the line heat source theory, but the sensor is even more robust than the LNP03 sensor. The heating and measurement properties are the same as for the LNP03 sensor. For the heating a constantan wire is embedded in the needle, which extends over the whole needle length. The temperature response to heating is measured with three Pt1000 RTDs placed at the following positions, (see Fig. 6): close to the tip, in the center of the needle and close to the base of the needle. The conversion of the resistance values measured by

20   the RTDs to temperature values is described in Sect. 3.1. As for LNP03, only the values of the middle sensor were used for evaluation and the temperature was measured with a 4-wire technique to increase measurement accuracy.

Figure 5. LNP04 thermal conductivity probe prototype. (Hukseflux, 2013)
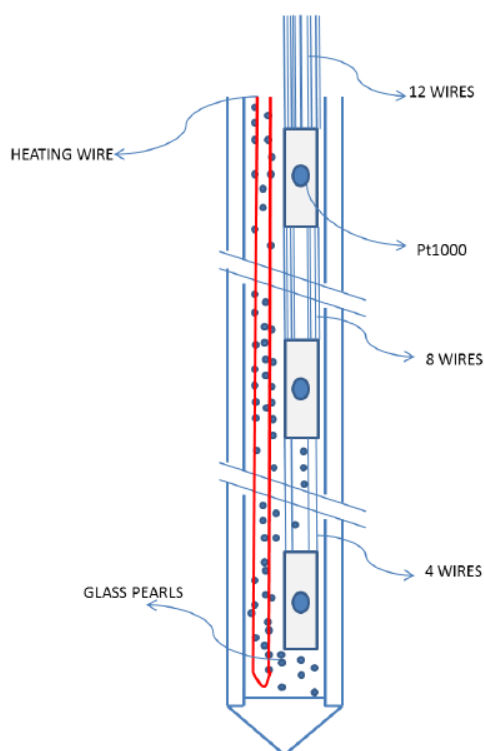
Figure 6. Sketch of the LNP04 sensor, showing its internal construction.

(Hukseflux, 2013)

4   Thermal conductivity measurements

In this section all measurements conducted with the TP02, the LNP03 and the LNP04 probes are described and the respective measured thermal conductivity values for the different sample materials are listed. Additionally the conductivities evaluated from the measurements with the LNP03 sensor are compared to those evaluated from the measurements with the LNP04 sensor. The main difference between these two types of sensors is their length and therefore the length-to-diameter ratio. Thus

the effect of that change in geometry on the evaluation of thermal conductivity can be studied by comparing their measurement results.

For the analysis the thermal model explained in Sect. 2.1.2, considering a heat source with thermal surface resistance and non-ideal properties, was used. The thermal conductivity was evaluated using the following standard procedure, as illustrated in Fig. 7:

1. Removal of any temperature trend from the data not associated to the active heating of the sensor.

2. Identification of the suitable interval of the measured temperature profile (linear part on the T-$\ln t$ graph).

3. Calculation of the thermal conductivity using the method of linear regression as described in Sect. 2.2.
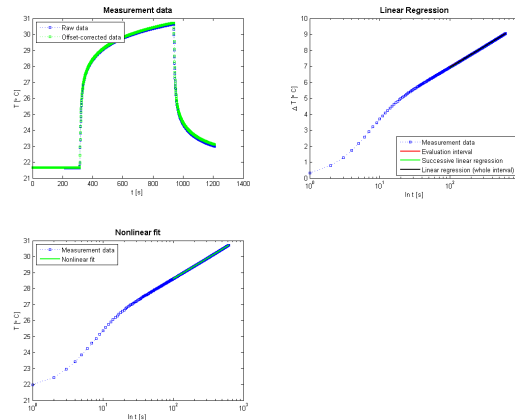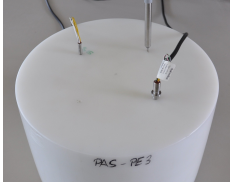
Figure 7. Thermal conductivity evaluation procedure performed in an agar sample with the LNP04 sensor with a heating time of 600 s and a heating power of 1 W as an example, evaluated and plotted by the software MATLAB. Top left: raw data and offset-corrected data of the total measurement (0 s to 300 s: phase before heating, used for the evaluation of the offset; 300 s to 900 s: heating phase, used for the evaluation of the thermal conductivity; 900 s to 1200 s: decline phase, which is not used for any evaluation). Bottom left: semi-logarithmic plot of the heating phase with the interval used for the linear fit shown in green. Top right: semi-logarithmic plot of the heating phase with the interval used for evaluation and successive and linear regression.

The commercial TP02 sensor as well as the prototypes LNP03 and LNP04 were tested by performing measurements in different

10 materials of well known thermal conductivity and compared to tabulated values. All measurements were performed under atmospheric pressure, at room temperature (21 °C to 24 °C) and a relative humidity of around 40 %, except for those in water ice, where the sample was stored in a deep-freezer at -20 °C. The materials used for the measurements are summarized in Table 3. The determination of the physical properties of a bulk of granular material, as needed for the glassbeads samples, is described in Appendix A.

15 In the following the measured thermal conductivity of each sample material is listed, where k_{mean} is the arithmetic mean, k_{median} the median of the measured thermal conductivities and the minimum and maximum conductivity values are denoted

Table 3. Overview of the sample materials.

Material		Properties
Agar		**Physical properties:** (Water at 20°C) Thermal conductivity k: $0.60\,\mathrm{Wm^{-1}K^{-1}}$ Heat capacity c_p: $4.18\,\mathrm{kJkg^{-1}K^{-1}}$ Density ρ: $998.21\,\mathrm{kgm^{-3}}$ **Dimensions:** 30 x 30 cm (D x H) **Medium:** Agar-water mixture
Glassbeads		
0.25 – 0.50 mm		**Physical properties:** Thermal conductivity k: $0.19\,\mathrm{Wm^{-1}K^{-1}}$ Heat capacity c_p: $1.201\,\mathrm{kJkg^{-1}K^{-1}}$ Bulk density ρ_{bulk}: $1510\,\mathrm{kgm^{-3}}$ **Dimensions:** 30 x 40 cm (D x H) **Medium:** Soda lime glass
1.00 – 1.25 mm		**Physical properties:** Thermal conductivity k: $0.19\,\mathrm{Wm^{-1}K^{-1}}$ Heat capacity c_p: $1.195\,\mathrm{kJkg^{-1}K^{-1}}$ Bulk density ρ_{bulk}: $1470\,\mathrm{kgm^{-3}}$ **Dimensions:** 35 x 28 x 30 cm (L x H x W) **Medium:** Soda lime glass
3.80 – 4.30 mm		**Physical properties:** Thermal conductivity k: $0.19\,\mathrm{Wm^{-1}K^{-1}}$ Heat capacity c_p: $1.193\,\mathrm{kJkg^{-1}K^{-1}}$ Bulk density ρ_{bulk}: $1450\,\mathrm{kgm^{-3}}$ **Dimensions:** 26 x 28 cm (D x H) **Medium:** Soda lime glass
Kerafol KP96		**Physical properties:** Thermal conductivity k: $2.40\,\mathrm{Wm^{-1}K^{-1}}$ Density ρ: $2600\,\mathrm{kgm^{-3}}$ **Dimensions:** 16 x 17 cm (D x H) **Medium:** Thermally conductive grease
PE		**Physical properties:** Thermal conductivity k: $0.41\,\mathrm{Wm^{-1}K^{-1}}$ Heat capacity c_p: $1.70\text{–}2.40\,\mathrm{kJkg^{-1}K^{-1}}$ Density ρ: $950\,\mathrm{kgm^{-3}}$ **Dimensions:** 30 x 18.5 cm (D x H) **Medium:** High-density polyethylene
Water ice		**Physical properties:** (Water ice at -20°C) Thermal conductivity k: $2.33\,\mathrm{Wm^{-1}K^{-1}}$ Heat capacity c_p: $1.94\,\mathrm{kJkg^{-1}K^{-1}}$ Density ρ: $919.40\,\mathrm{kgm^{-3}}$ **Dimensions:** 26 x 25 cm (D x H) **Medium:** Water ice

as k_{min} and k_{max}, respectively. The absolute measurement error $|\delta k|$ is the mean value of the estimated errors of the single measurements, determined according to Eq. (33), while σ is the mean value of the standard deviations of the single measurements, calculated by Eq. (35). The values of the used LNP03 and LNP04 needles are listed separately.

4.1 Agar

5   All three sensor types, TP02, LNP03 and LNP04, were used for the measurements in agar. The same sample was used for all sensors. Enough sample material was produced to allow for degradation of the penetrated layer after a measurement with one sensor and use the untouched sample surface for the other sensor probes. The disadvantage of this method is that one cannot rule out that invisible small cracks occur at the sample surface by the insertion of a sensor. If this happens the contact between sensor and medium is getting worse. The better, but much more time-consuming method, would be to produce a new sample

10   for each probe and put the probes into the agar before it solidifies.

The thermal conductivities determined by the different sensors are summarized in Table 4 and shown in Fig. 8 versus the chronologically ordered measurements.

Table 4. Thermal conductivity of agar determined by the TP02, the LNP03 and the LNP04 sensor.

Sensor	No.	$\mathbf{k_{mean}}$	$\mathbf{k_{median}}$	σ	$\mathbf{|\delta k|}$	$\mathbf{k_{min}}$	$\mathbf{k_{max}}$
				$\mathrm{Wm^{-1}K^{-1}}$			
TP02	5	0.575	0.601	0.041	0.064	0.489	0.631
LNP03							
needle 2	5	0.609	0.604	-	0.023	0.603	0.623
needle 3	5	0.608	0.603	-	0.024	0.602	0.627
needle 4	5	0.601	0.596	-	0.023	0.592	0.613
all	15	0.609	0.604	0.010	0.023	0.592	0.627
LNP04							
needle 1	5	0.622	0.615	-	0.024	0.611	0.636
needle 2	5	0.592	0.590	-	0.023	0.587	0.604
needle 3	5	0.619	0.615	-	0.024	0.609	0.632
needle 4	5	0.642	0.643	-	0.024	0.626	0.653
all	20	0.618	0.615	0.021	0.024	0.587	0.653

$$\mathbf{k_{tabulated} = 0.60 \pm 10\% \; Wm^{-1}K^{-1}}$$
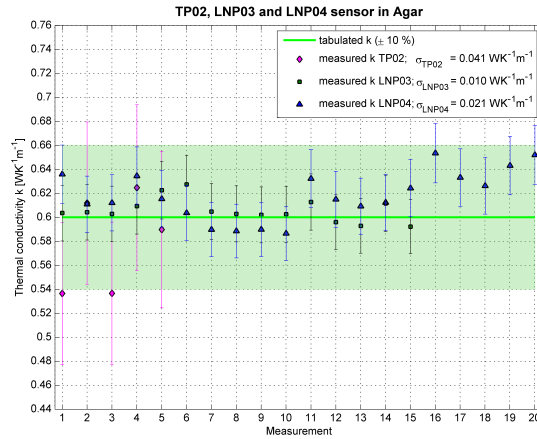
Figure 8. Thermal conductivity values of agar, measured by the TP02, LNP03 and LNP04 sensor. The error bars are representing the measurement error as described in Sect. 2.2.2 for each measurement value. The green line indicates the tabulated value of the thermal conductivity (Hukseflux, 2007) with a range of ±10 %. In the legend the standard deviation σ, determined according to Eq. (35), of the respective measurement sequence is given.

4.2 Glassbeads

Three different single grain size fractions were investigated. Glassbeads of 0.25 mm to 0.50 mm grain size were used for measurements with the TP02, LNP03 and LNP04 sensor. Thermal conductivity measurements in the glassbeads with a grain size of 1.00 mm to 1.25 mm and 3.80 mm to 4.30 mm were performed only with the TP02 sensor.

5   The thermal conductivity values are summarized in Tables 5, 6 and 7 for the different sizes of the glassbeads, respectively. A comparison of the conductivities determined by all three sensors in the smallest glassbeads is shown in Fig. 9. Having a look on the values measured by the TP02 sensor in the different sizes of glassbeads (see Fig. 10) an increase of thermal conductivity with increasing grain size can be observed. This was already described by (Hütter, 2011). The reason for the correlation between bead size and conductivity is that the heat transfer via the gas phase is much more effective than via the

10   contact points of the solid grains. When applied to regoliths under very low pressure or vacuum, grain to grain contacts become increasingly important.

Table 5. Thermal conductivity of glassbeads with a grain size of 0.25 mm to 0.50 mm determined by the TP02, the LNP03 and the LNP04 sensor. The value for $k_{tabulated}$ is the thermal conductivity of a bulk of glassbeads.

Sensor	No.	$\mathbf{k_{mean}}$	$\mathbf{k_{median}}$	σ	$|\delta\mathbf{k}|$	$\mathbf{k_{min}}$	$\mathbf{k_{max}}$
				$\mathrm{Wm^{-1}K^{-1}}$			
TP02	10	0.164	0.163	0.012	0.018	0.141	0.188
LNP03							
needle 2	5	0.206	0.205	-	0.008	0.205	0.209
needle 3	5	0.204	0.203	-	0.008	0.200	0.207
needle 4	5	0.206	0.206	-	0.008	0.206	0.208
all	15	0.205	0.206	0.002	0.008	0.200	0.209
LNP04							
needle 1	5	0.203	0.203	-	0.008	0.200	0.210
needle 2	5	0.206	0.205	-	0.008	0.198	0.213
needle 3	5	0.213	0.213	-	0.008	0.209	0.217
needle 4	5	0.211	0.208	-	0.008	0.207	0.216
all	20	0.209	0.209	0.006	0.008	0.198	0.217

$$\mathbf{k_{tabulated} = 0.19 \pm 10\% \ Wm^{-1}K^{-1}}$$

Table 6. Thermal conductivity of glassbeads with a grain size of 1.00 mm to 1.25 mm determined by the TP02 sensor. The value for $k_{tabulated}$ is the thermal conductivity of a bulk of glassbeads.

Sensor	No.	$\mathbf{k_{mean}}$	$\mathbf{k_{median}}$	σ	$|\delta\mathbf{k}|$	$\mathbf{k_{min}}$	$\mathbf{k_{max}}$
				$\mathrm{Wm^{-1}K^{-1}}$			
TP02	5	0.176	0.180	0.012	0.019	0.159	0.192

$$\mathbf{k_{tabulated} = 0.19 \pm 10\% \ Wm^{-1}K^{-1}}$$

Table 7. Thermal conductivity of glassbeads with a grain size of 3.80 mm to 4.30 mm determined by the TP02 sensor. The value for $k_{tabulated}$ is the thermal conductivity of a bulk of glassbeads.

Sensor	No.	$\mathbf{k_{mean}}$	$\mathbf{k_{median}}$	σ	$\mathbf{|\delta k|}$	$\mathbf{k_{min}}$	$\mathbf{k_{max}}$
				$\mathrm{Wm^{-1}K^{-1}}$			
TP02	5	0.192	0.196	0.026	0.021	0.159	0.226
			$\mathbf{k_{tabulated} = 0.19 \pm 10\%\ Wm^{-1}K^{-1}}$				
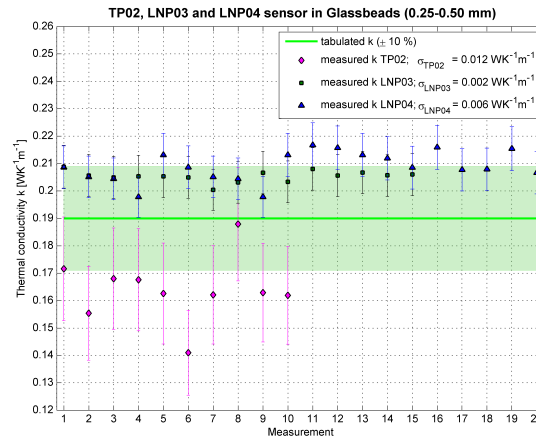
Figure 9. Thermal conductivity values of glassbeads with a grain size of 0.25 mm to 0.50 mm, measured by the TP02, LNP03 and LNP04 sensor. The tabulated value of the thermal conductivity (Hukseflux, 2013) refers to a bulk of glassbeads and is indicated by the green line with a range of $\pm 10\%$. The error bars are representing the measurement error as described in Sect. 2.2.2 for each measurement value. In the legend the standard deviation σ, determined according to Eq. (35), of the respective measurement sequence is given.

4.3 Kerafol KP96

The thermal grease Kerafol KP96 was used for measurements with the TP02, LNP03 and LNP04 sensor. This highly viscous grease was stirred well before conducting the measurements in order to get a homogeneous medium. Despite slow and careful stirring some air bubbles emerged in the fluid which might affect the measurement of the thermal conductivity. Thus, after stirring the sensor was put into the grease carefully and before starting the measurements it was waited some time and slightly tapped against the sample container, so that most of the bubbles were able to rise to the surface and to escape.

The thermal conductivities determined by the different sensors are summarized in Table 8 and shown in Fig. 11. In the upper panel it can be seen that the measured thermal conductivity is far below the value given by the manufacturer. Maybe the reason for this high deviation is that the thermal conductivity value given by the manufacturer is only valid when this thermal grease
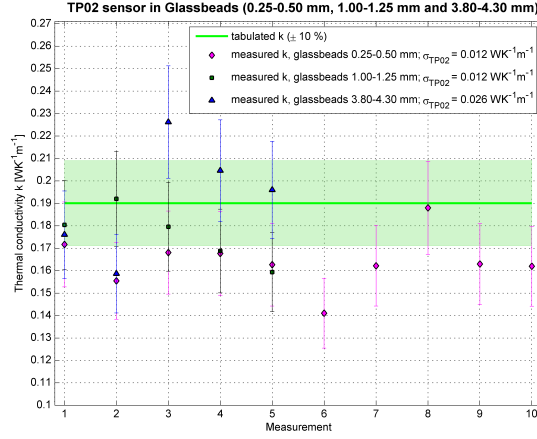
Figure 10. Thermal conductivity values of glassbeads in the different size fractions determined by the TP02 sensor. The error bars are representing the measurement error as described in Sect. 2.2.2 for each measurement value. The green line indicates the tabulated value of the thermal conductivity (of a bulk of glassbeads) (Hukseflux, 2013) with a range of ± 10 %. In the legend the standard deviation σ, determined according to Eq. (35), of the respective measurement sequence is given.

is applied in a thin contact layer and not in the bulk fluid, as used for our measurements. This fact was already observed in the previous measurements described by (Kömle et al., 2013).

Table 8. Thermal conductivity of Kerafol KP96 determined by the TP02, the LNP03 (needle 2) and the LNP04 sensor.

Sensor	No.	k_{mean}	k_{median}	σ	$|\delta k|$	k_{min}	k_{max}
				$Wm^{-1}K^{-1}$			
TP02	7	0.858	0.870	0.027	0.049	0.815	0.888
LNP03	5	0.968	0.964	0.011	0.038	0.962	0.989
LNP04							
needle 2	5	0.912	0.901	-	0.035	0.867	0.987
needle 3	5	0.982	0.980	-	0.038	0.977	0.993
all	10	0.947	0.978	0.048	0.036	0.867	0.993

$$k_{tabulated} = 2.40 \pm 10\% \ Wm^{-1}K^{-1}$$
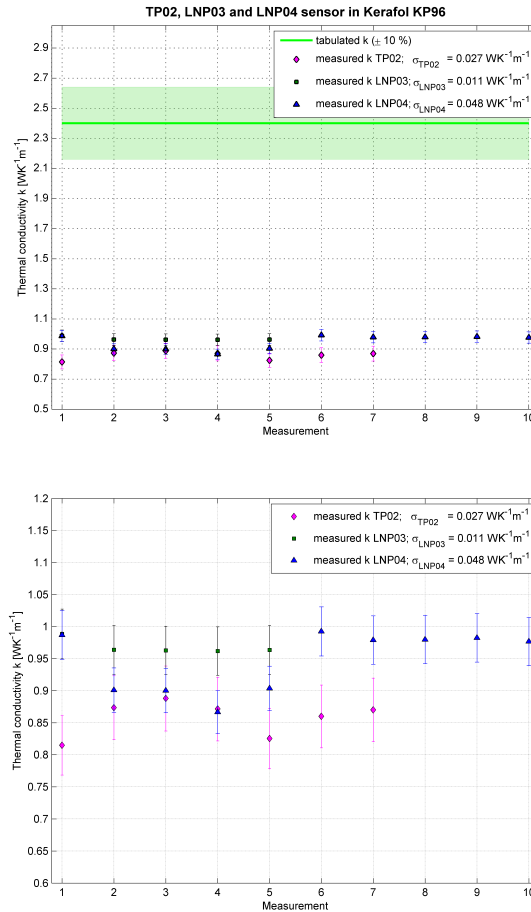
Figure 11. Thermal conductivities of the thermal grease Kerafol KP96 measured by the TP02, LNP03 and LNP04 sensors. In the upper panel green line indicates the value of the thermal conductivity given by the manufacturer (Kerafol, 2013) with a range of $\pm 10\,\%$. The lower picture shows the range of the measured values in more detail. The error bars are representing the measurement error as described in Sect. 2.2.2 for each measurement value. In the legend the standard deviation σ, determined according to Eq. (35), of the respective measurement sequence is given.

4.4 PE – Polyethylene

All three sensors, TP02, LNP03 and LNP04, were used for the measurements in PE. The sensors were inserted into predrilled holes with different diameters and lengths, to provide proper fitting. The hole for the TP02 has a diameter of 1.8 mm and a length of 150 mm, the one for the LNP03 and LNP04 a diameter of 3.6 mm and a length of 115 mm. For improvement of the thermal contact between sensor and sample Glycerin was used as a contact fluid. The thermal conductivity of Glycerin is around $0.3\ \mathrm{Wm^{-1}K^{-1}}$ and so significantly higher than that of air, which is $0.026\ \mathrm{Wm^{-1}K^{-1}}$.

The thermal conductivities determined by the different sensors are summarized in Table 9 and shown in Fig. 12.

Table 9. Thermal conductivity of PE determined by the TP02, the LNP03 and the LNP04 sensor.

Sensor	No.	$\mathrm{Wm^{-1}K^{-1}}$					
		$\mathbf{k_{mean}}$	$\mathbf{k_{median}}$	σ	$|\delta\mathbf{k}|$	$\mathbf{k_{min}}$	$\mathbf{k_{max}}$
TP02	5	0.429	0.425	0.043	0.044	0.370	0.478
LNP03							
needle 2	5	0.473	0.473	-	0.015	0.469	0.479
needle 3	5	0.466	0.467	-	0.014	0.464	0.467
needle 4	5	0.469	0.471	-	0.015	0.459	0.477
all	15	0.469	0.469	0.005	0.015	0.459	0.479
LNP04							
needle 2	5	0.453	0.454	-	0.014	0.443	0.461
needle 3	5	0.467	0.467	-	0.015	0.464	0.471
all	10	0.460	0.463	0.009	0.015	0.443	0.471
		$\mathbf{k_{tabulated} = 0.41 \pm 10\%\ Wm^{-1}K^{-1}}$					
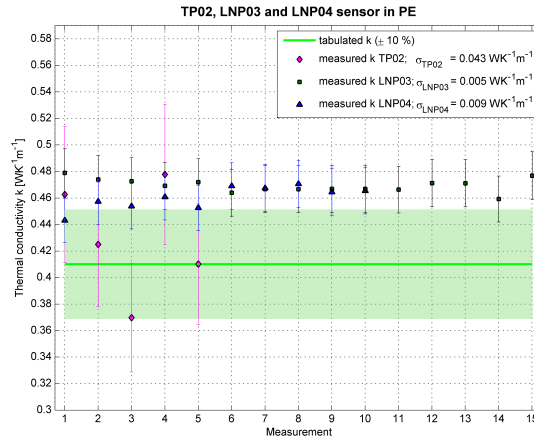
Figure 12. Thermal conductivities of the solid plastic material PE measured by the TP02, LNP03 and LNP04 sensor. The tabulated value of the thermal conductivity (Faigle, 2014) is indicated by the green line with a range of $\pm 10\%$. The error bars are representing the measurement error as described in Sect. 2.2.2 for each measurement value. In the legend the standard deviation σ, determined according to Eq. (35), of the respective measurement sequence is given.

4.5 Water ice

Water ice was used for measurements with the TP02, LNP03 and LNP04 sensor. No fissures or even cracks were observed after freezing. This suggests that there was a good contact between sensor and sample material, which is consistent with the low variability of the thermal conductivity values determined by all sensors and the good agreement with the tabulated value.

5   The thermal conductivities determined by the different sensors are summarized in Table 10 and shown in Fig. 13.

Table 10. Thermal conductivity of water ice determined by the TP02, the LNP03 (needle 2) and the LNP04 (needle 2) sensor.

Sensor	No.	k_{mean}	k_{median}	σ	$|\delta k|$	k_{min}	k_{max}
				$\mathrm{Wm^{-1}K^{-1}}$			
TP02	5	2.260	2.248	0.053	0.072	2.187	2.315
LNP03	5	2.297	2.272	0.05	0.074	2.263	2.392
LNP04	5	2.290	2.288	0.055	0.072	2.228	2.354

$$\mathbf{k_{tabulated} = 2.33} \pm 10\% \ \mathrm{Wm^{-1}K^{-1}}$$
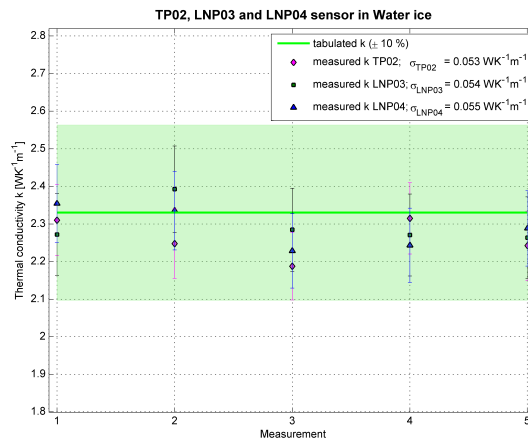
Figure 13. Thermal conductivity values of water ice determined by the TP02, LNP03 and LNP04 sensor. The error bars are representing the measurement error as described in Sect. 2.2.2 for each measurement value. The green line indicates the tabulated value of the thermal conductivity of water ice at -20 °C (Wikipedia, 2014) with a range of ± 10 %. In the legend the standard deviation σ, determined according to Eq. (35), of the respective measurement sequence is given.

5 Calibration of the LNP sensors

The custom-made thermal conductivity sensors LNP03 and LNP04 are rugged prototype sensors. As already mentioned in (Kömle et al., 2013) these sensors are necessarily thicker and shorter and so cannot fulfil the requirements for the evaluation of the thermal conductivity by Eq. (8). Thus, there are in principle two possibilities to do this. Either one can use a much more complicated formalism, applying the theory of non-ideal (short and thick) sensors, or one uses the simple theory of ideal sensors with an additional calibration function. While the first method has been described in (Hütter, 2011), (Hütter and Kömle, 2012) and (Macher et al., 2013), the second method is described in this section. The testing and calibration of the LNP03 sensor was already conducted by (Kömle et al., 2013) and now verified by measurements in partly different sample materials and an adapted measurement setup. Calibration of the LNP04 sensor was carried out in the same way. As reference sensor an off-the-shelf thermal conductivity probe TP02 was used. A detailed description of all the sensors was given in Sect. 3.

5.1 Characterization of calibration samples

For the calibration measurements the used materials have been selected in order to cover the range of thermal conductivities from around $0.01\ \mathrm{Wm^{-1}K^{-1}}$ to around $2\ \mathrm{Wm^{-1}K^{-1}}$. All measurements for the calibration of the LNP sensors were performed under atmospheric pressure at temperatures in the range of 21 °C to 24 °C and a humidity around 40 %. The lower end, around $0.10\ \mathrm{Wm^{-1}K^{-1}}$, corresponds to granular materials. As a representative of such a material silica glassbeads with a grain size in the range of 0.25 mm to 0.5 mm were used. For thermal conductivity of about $0.40\ \mathrm{Wm^{-1}K^{-1}}$ the solid plastic material PE and for the range of $0.50\ \mathrm{Wm^{-1}K^{-1}}$ to $0.60\ \mathrm{Wm^{-1}K^{-1}}$ water, respectively agar, were used as sample material. Investigation of the upper end of the range of thermal conductivity we were interested in, around $2\ \mathrm{Wm^{-1}K^{-1}}$, was performed by using compact water ice. For that, water was placed into a deep-freezer with the measurement needles inserted and cooled down over several days until a constant temperature of about -20 °C was reached. Despite the slight expansion of the sample due to freezing no visible cracks were formed during the freezing process, which could have affected the thermal contact of the needles with the sample. The used container was flexible and allowed expansion of the ice during freezing both towards the sides and in upward direction. There was no danger of local phase changes of the sample material along the contact surface of sensor and sample, because temperature changes due to sensor heating never exceeded a few degrees. To cover the range around $1\ \mathrm{Wm^{-1}K^{-1}}$ and to bridge the gap between water/agar and water ice the thermally conductive grease Kerafol KP96 was used. It is a viscous fluid, so convection is suppressed, but it is soft enough, so that the sensors can be inserted easily.

5.2 Calibration strategy

For the calibration the following steps were performed:

1. Reasonably large-sized samples were prepared, which were big enough in diameter and height for the respective sensor. This made sure that no influence from the sample boundaries could disturb the measurements. Estimating the minimum sample sizes can be done by means of the formulae given in (Hütter and Kömle, 2012).

2. The samples (with sensors inserted) were kept for at least several hours in a thermally stable environment to ensure isothermal conditions for the measurements. All measurements were performed at room temperature, i.e. at an ambient temperature range of 21 °C to 24 °C, except of those in water ice, where the sample was stored in a deep-freezer at -20 °C.

3. For the thermal conductivity measurements each sensor was heated separately. To make sure that the sample is in thermal equilibrium again after one measurement, there were long enough time periods between two subsequent measurements (several hours). The heating periods of the sensors are depending on the sample and were in the range of 300 s to 600 s.

4. Evaluation of the thermal conductivity was performed as described in Sect. 4.

The thermal conductivity results determined from TP02 measurements are listed in Table 11 and those determined from LNP03 and LNP04 measurements in Table 12.

Table 11. Thermal conductivity measurement results for the TP02 sensor in different sample materials.

Sensor	Thermal conductivity k [$\mathrm{Wm^{-1}K^{-1}}$]				
	Glassbeads	**PE**	**Agar**	**KP96**	**Water ice**
TP02	0.172	0.463	0.537	0.815	2.310
	0.155	0.425	0.612	0.874	2.248
	0.168	0.370	0.537	0.888	2.187
	0.168	0.478	0.625	0.872	2.315
	0.163	0.410	0.590	0.825	2.242
	0.141	-	-	0.860	-
	0.162	-	-	0.870	-
	0.188	-	-	-	-
	0.163	-	-	-	-
	0.162	-	-	-	-
mean	**0.164**	**0.429**	**0.580**	**0.858**	**2.260**
tabulated	0.19	0.41	0.60	2.40	2.33

5.3 Calibration results

The mean value of the individual results from all three sensors was used to evaluate the calibration factors for the different samples, shown in Table 13. So the true thermal conductivity can be obtained from a measurement with the prototype LNP sensor according to formula:

$$k_{TP02} = f_{cal} \cdot k_{LNP} \tag{39}$$

The average value calculated from the individual calibration factors is designated as f_{cal} and given in Table 13 too.

Table 12. Thermal conductivity measurement results for the LNP03 and the LNP04 sensor in different sample materials.

Sensor	Thermal conductivity k [Wm^{-1}K^{-1}]				
	Glassbeads	**PE**	**Agar**	**KP96**	**Water ice**
LNP03	0.209	0.479	0.604	0.989	2.272
	0.206	0.474	0.604	0.964	2.393
	0.205	0.473	0.603	0.963	2.285
	0.205	0.469	0.609	0.962	2.271
	0.205	0.472	0.623	0.964	2.263
	0.205	0.464	0.627	-	-
	0.200	0.467	0.605	-	-
	0.203	0.467	0.603	-	-
	0.207	0.467	0.602	-	-
	0.203	0.467	0.603	-	-
	0.208	0.466	0.613	-	-
	0.206	0.472	0.596	-	-
	0.207	0.471	0.593	-	-
	0.206	0.459	0.612	-	-
	0.206	0.477	0.592	-	-
mean	**0.205**	**0.469**	**0.606**	**0.968**	**2.297**
LNP04	0.209	0.443	0.636	0.987	2.354
	0.205	0.457	0.611	0.901	2.335
	0.204	0.454	0.612	0.900	2.228
	0.198	0.461	0.634	0.867	2.243
	0.213	0.453	0.615	0.904	2.288
	0.209	0.469	0.604	0.993	-
	0.205	0.467	0.590	0.979	-
	0.204	0.471	0.589	0.980	-
	0.198	0.464	0.590	0.983	-
	0.213	0.465	0.587	0.977	-
	0.217	-	0.632	-	-
	0.216	-	0.615	-	-
	0.213	-	0.609	-	-
	0.212	-	0.612	-	-
	0.209	-	0.624	-	-
	0.216	-	0.653	-	-
	0.208	-	0.633	-	-
	0.208	-	0.626	-	-
	0.215	-	0.643	-	-
	0.207	-	0.652	-	-
mean	**0.209**	**0.460**	**0.618**	**0.947**	**2.290**
tabulated	0.19	0.41	0.60	2.40	2.33

Table 13. Calibration factors derived for the different materials.

Sensor	Calibration factor [1]					
	Glassbeads	**PE**	**Agar**	**KP96**	**Water ice**	**f$_{cal}$**
LNP03–TP02	0.799	0.914	0.957	0.886	0.984	**0.908**
LNP04–TP02	0.786	0.932	0.938	0.906	0.987	**0.909**

In Fig. 14 the conductivities measured by the LNP sensors versus that of the TP02 reference sensor can be seen. The symbols represent the mean values listed in Tables 11 and 12, while the dotted lines are a linear fit through these measured values, respectively.
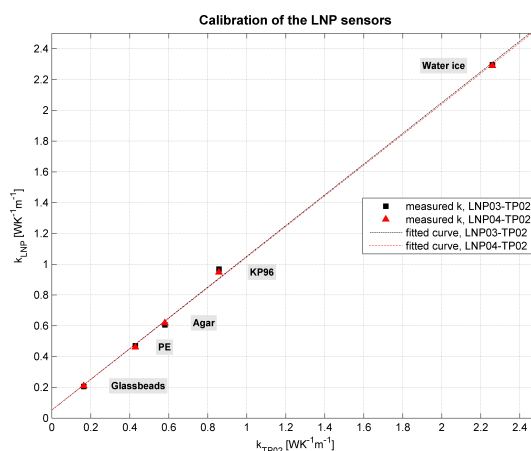
Figure 14. Calibration of the prototypes LNP03 and LNP04 with the commercial TP02 thermal conductivity sensor, which is used as a reference sensor for the calibration measurement. The red symbols represents the mean measurement values of the respective sensor and the dotted line is a linear fit to them.

6 Comparison between the LNP03 and LNP04 sensor

The LNP03 and the LNP04 only differ in sensor length. While the LNP03 sensor has a length of 100 mm, the LNP04 sensor is only 80 mm long. This means a length-to-diameter ratio of 22 for the LNP04 sensor instead of 28 for the LNP03, and thus a geometry which is less optimal with respect to line heat source theory.

In this section potential differences in thermal conductivity values, measured by the LNP03 and the LNP04, are shown. All evaluated conductivities measured in the various sample materials are listed in Table 12. The average value of each sample is written in bold. In Fig. 15 these mean conductivities obtained from the two different sensors, which are represented by the symbols, were plotted against each other, while the dotted line is a linear fit through the data points. From the mean values a

conversion factor between the LNP03 and LNP04 sensor was calculated, shown in Table 14. So the following relation can be formulated:

$$k_{LNP03} = f_{con} \cdot k_{LNP04} \tag{40}$$

These conversion factors versus the thermal conductivities measured by the LNP04 sensor are plotted in Fig. 16. A factor of 5 1 is indicated by a bold line with a $\pm 3 \%$ interval (shaded area). All conversion factors lie within this range. No trend of the factors is apparent for the different sample materials. Thus it can be assumed that the difference in length between the LNP03 and the LNP04 sensor does not have a significant effect on the determination of the thermal conductivity (as long as the heating periods are not too long).
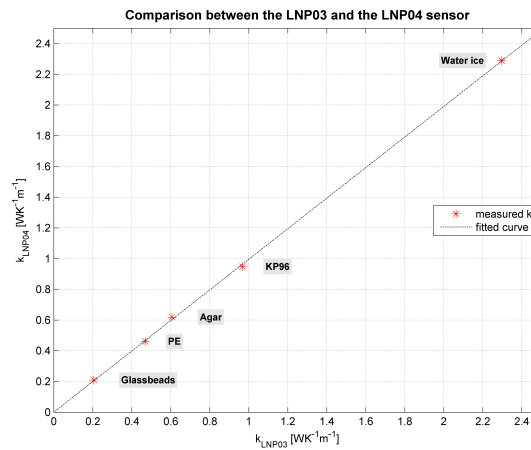
Figure 15. Comparison between the prototype LNP03 and the LNP04 thermal conductivity sensor. The symbols represents the mean measurement values of the LNP03 and the LNP04 sensor, while the dotted line is a linear fit through the data points.

Table 14. Conversion factors derived for the different materials.

Sensor	Conversion factor [1]					
	Glassbeads	**PE**	**Agar**	**KP96**	**Water ice**	$\mathbf{f_{con}}$
LNP03–LNP04	0.983	1.020	0.980	1.022	1.003	**1.002**

7   Conclusions

10 In the course of this work various investigations concerning thermal conductivity measurements with two different types of ruggedized, mathematically non-ideal sensors were made. In a first step the thermal conductivity of different samples was
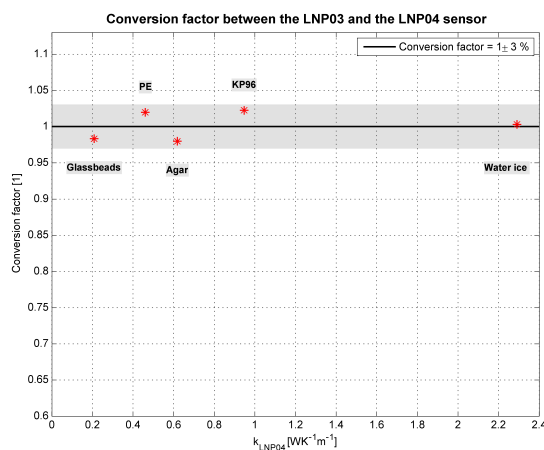
Figure 16. Plot of the conversion factors versus the thermal conductivities measured by the LNP04 sensor for the different sample materials. The bold line indicates a conversion factor of 1. Around this line a ±3 % interval shows the scattering area of the factors for the different materials.

determined by the LNP03 as well as by the shorter LNP04 thermal conductivity probe. Due to the mathematically non-ideal geometry of the LNP03 and the LNP04 it was necessary to calibrate them. The LNP03 sensor has already been calibrated by (Kömle et al., 2013), but it was done again with an improved measurement setup, while the LNP04 was calibrated for the first time. The off-the-shelf TP02 thermal conductivity sensor serves as a reference. An average calibration factor $f_{cal} = 0.908$ for

5 the LNP03 and $f_{cal} = 0.909$ for the LNP04 was found. This is closer to 1 (the reference sensor TP02) as found by (Kömle et al., 2013) for the LNP03, which was $f_{cal} = 0.80$. The main focus of this work is the influence of the probe geometry of non-ideal sensors on measurement results. Thus, the conductivities measured by the LNP03 and the LNP04 probes were compared to each other. By performing measurements with both sensors in various sample materials a conversion factor could be calculated for each sample. The average conversion factor is $f_{con} = 1.002$ and the single conversion factors lie within a ±3 % range.

10 These results show that there is no significant difference between the conductivities determined by the different LNP probes and confirm that the probe geometry of the rugged non-ideal prototype sensors doesn't have significant influence on thermal conductivity values, provided the derived calibration factors are applied.

It can be noticed that both the measurement uncertainties and the variance in the data are larger for TP02 data than for the data determined by the LNP sensors. This can be explained by having a look at the calculation of the measurement error

15 by Eq. (33), which includes the influence of the resistance of the heating wire, the heating current error and the temperature error. Since the TP02 is a thin and long sensor much less heating current is needed to provide proper temperature data for the evaluation as for the LNP sensors, what leads to a larger relative heating current error. Additionally the temperature increase in the TP02 while heating is much less than in the LNP sensors, thereby causing a larger relative temperature error. However, the TP02 performs better with regard to certain systematic errors (bias) which haven't been considered in our model:

- Heat drain through measurement leads.

- Non-ideal geometry (especially finite probe radius and finite probe length) as assumed by the linear T-$\ln t$ evaluation formula.

The smaller temperature increase in TP02 ensures that the heat drain through the measurement leads is mostly negligible for this sensor, in contrast to the LNP. Furthermore, since the geometry of the TP02 almost represents a perfect line heat source it is better described by the used theoretical model than the LNP03 and the LNP04. Thus, in spite of its smaller precision the TP02 is a reference in this context due to the reduction of the mentioned systematic errors (apart from applications to coarse-grained granular media).

Appendix A: Heat transfer in granular media

In this section systems consisting of grainy solid material with small voids in between are discussed. *Regolith*, a granular and porous material including dust, soil and broken rock, is such a system. Planetary bodies, like the Moon, Mars, asteroids and comets, which are of interest for *in situ* thermal conductivity measurements and therefore for this work, are covered by layers of regolith. In space the voids between the particles are empty due to the vacuum conditions, whereas under atmospheric pressure these voids are filled with gas.

Particulate systems are characterized by so-called *effective properties*, which are determined by averaging the properties of the single components (solid and fluid) over the volume. The *effective thermal conductivity*, k_{eff}, comprises all modes of heat transfer (conduction, radiation and convection). It is the value that can be measured directly by thermal conductivity probes. The effective thermal conductivity is a function of the contributing individual conductivities (Hütter, 2011):

$$k_{eff} = f(k_s, k_g, k_{sg}, k_{sc}, k_{rad}, k_{conv}) \tag{A1}$$

where k_s and k_g are the solid phase and gas phase conductivities, respectively, k_{sg} describes the heat transport between solid and gas phase and k_{sc} the heat transfer between the particles. The radiative heat transfer is expressed as k_{rad} and the convective heat transfer in the voids as k_{conv}. The evaluation of the respective contribution of the single conductivities is pretty complex and not further discussed here. Another effective property of such a system is the *effective specific heat capacity*, which can be calculated by the following formula:

$$c_p^{eff} = \psi \cdot c_p^{void} + (1 - \psi) \cdot c_p^{solid} \tag{A2}$$

where c_p^{void} and c_p^{solid} are the specific heat capacities of the voids between the particles and of the solid medium, respectively. The parameter ψ is called porosity and defined in the following.

Porosity is the ratio of the void-space volume and the total volume of the material:

$$\psi = \frac{V_{void}}{V_{total}} = \frac{V_{void}}{V_{solid} + V_{void}} \tag{A3}$$

A relation between porosity and density can be given as follows:

$$\psi = 1 - \frac{\rho_{bulk}}{\rho_{solid}} \tag{A4}$$

where ρ_{bulk} is the *bulk density* of the total granular medium and ρ_{solid} is the density of the solid phase alone. In a medium that contains particles of different grain size the porosity is always smaller than in a medium with equally sized particles, because

5 denser packing is possible (see Figure 17, detail A).

(2014) created by Schaffer A.

Convection
Thermal Conduction
Radiation
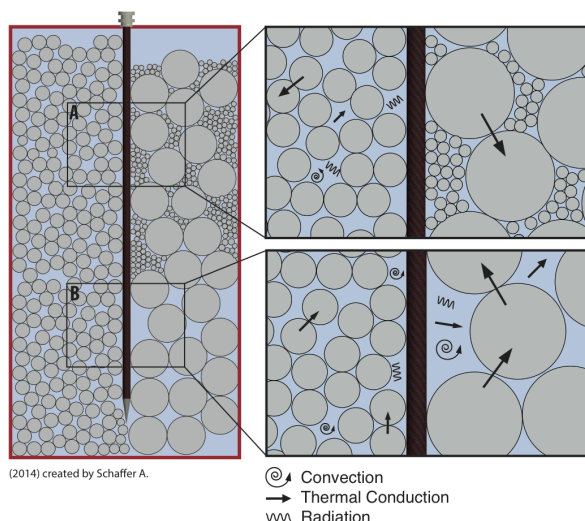
Figure 17. Modes of heat transfer in granular media. In the left picture a thermal conductivity probe, inserted into a medium with different particle sizes can be seen. On the right side of the probe detail A shows the heat transfer processes in a particulate system with different sized particles, whereas in detail B the heat transfer processes in a system with equally sized particles is shown. The light blue areas represent the voids. (Schaffer, 2014)

References

Abramowitz, M. and Stegun, I. A.: Handbook of mathematical functions with formulas, graphs and mathematical tables, U.S. Department of Commerce, National Bureau of Standards, 1964.

Agilent: Agilent 34970A/34972A data acquisition / switch unit users's guide, Agilent Technologies, 2012.

5 Blackwell, J.: Transient heat flow problems in cylindrical symmetry, Ph.D. thesis, University of Western Ontario, London, Canada, 1952.

Blackwell, J.: A transient-flow method for determination of thermal constants of insulating materials in bulk, Part 1 – Theory, Journal of Applied Physics, 25(2):137-144., doi:10.1063/1.1721592, 1954.

Carslaw, H. S. and Jaeger, J. C.: Conduction of heat in solids, Oxford University Press, 2nd edn., 1959.

ESA: Luna Mission Speed Dating, Russia-ESA Lunar Exploration Cooperation, 2014.

10 Faigle: Data sheet, Material: PAS-PE3, Faigle Kunststoffe GmbH, 2014.

Goodhew, S. and Griffiths, R.: Analysis of thermal-probe measurements using an iterative method to give sample conductivity and diffusivity data, Applied Energy, 77:205-223., doi:10.1016/S0306-2619(03)00122-3, 2004.

Heusler: Datenblatt ISOTAN, Isabellenhütte Heusler GmbH & Co. KG, 2014.

Hofmeister, A. M., Branlund, J. M., and Pertermann, M.: Treatise on Geophysics, Elsevier, 2007.

15 Hütter, E.: Development and testing of thermal sensors for planetary applications, Ph.D. thesis, University of Graz, 2011.

Hütter, E. and Kömle, N.: Performance of thermal conductivity probes for planetary applications, Geoscientific Instrumentation Methods and Data Systems, 1:53-75., doi:10.5194/gi-1-53-2012, 2012.

Hukseflux: TP08 - Small size non-steady-state probe for thermal conductivity measurement, User manual, Hukseflux Thermal Sensors, 2007.

Hukseflux: TP02 - Non-steady-state probe for thermal conductivity measurement, User manual, Hukseflux Thermal Sensors, 2010.

20 Hukseflux: LNP04 - Construction and functional tests v1304, Hukseflux Thermal Sensors, 2013.

Incropera, F. P., DeWitt, D. P., Bergman, T. L., and Lavine, A. S.: Fundamentals of heat and mass transfer, John Wiley & Sons, 6th edition edn., 2007.

Jaeger, J.: Conduction of heat in an infinite region bounded internally by a circular cylinder of a perfect conductor, Australian Journal of Physics, 9:167-179., doi:10.1071/PH560167, 1956.

25 Jones, B.: Thermal conductivity probe: Development of method and application to a coarse granular medium., Journal of Physics E: Scientific Instruments, 21:832-839., doi:10.1088/0022-3735/21/9/002, 1988.

Kerafol: Keratherm - Thermal grease, Kerafol Keramische Folien GmbH, 2013.

Kömle, N., Macher, W., Kargl, G., and Bentley, M.: Calibration of non-ideal thermal conductivity sensors, Geoscientific Instrumentation Methods and Data Systems, 2:151-156., doi:10.5194/gi-2-151-2013, 2013.

30 Kömle, N. I.: Solar-Planetary Relations, chap. Cometary surface processes: Experiments and theory, pp. 227–259, Research Signpost, Trivandrum, 2005.

Langseth, M. G. J., Clark, S. P. J., Chute, J. L. J., Kheim, S. J. J., and Wechsler, A. E.: Apollo 15: Preliminary science report (NASA SP-289), chap. Heat flow experiment, National Aeronautics and Space Administration (NASA), 1972.

Langseth, M. G. J., Kheim, S. J. J., and Chute, J. L. J.: Apollo 17: Preliminary science report (NASA SP-330), chap. Heat flow experiment,
35 National Aeronautics and Space Administration (NASA), 1973.

Macher, W., Kömle, N., Bentley, M., and Kargl, G.: The heated infinite cylinder with sheath and two thermal surface resistance layers, International Journal of Heat and Mass Transfer, 57:528-534., doi:10.1016/j.ijheatmasstransfer.2012.10.070, 2013.

McGee, T. D.: Principles and methods of temperature measurement, 1988.

Schaffer, A.: Calibration strategy for a thermal probe applicable in planetary research, Master's thesis, University of Graz, 2014.

TTi: TTi instruction manual, Thurlby Thandar Instruments Ltd., 2003.

Wikipedia: http://de.wikipedia.org/wiki/Wärmeleitfähigkeit, 2014.

5   Zent, A., Hecht, M., Cobos, D., Wood, S., Hudson, T., Milkovich, S., DeFlores, L., and Mellon, M.: Initial results from the thermal and
    electrical conductivity probe (TECP) on Phoenix, Journal of Geophysical Research, 115., doi:10.1029/2009JE003420, 2010.

Özisik, M. N.: Boundary value problems of heat conduction, Dover Phoenix Editions, 1989.